JOURNAL OF GEOPHYSICAL RESEARCH, VOL. 107, NO. B7, 2141, 10.1029/2001JB000493, 2002

Cataclastic slip band distribution in normal fault damage zones, Nubian sandstones, Suez rift

X. Du Bernard[1] and P. Labaume
Laboratoire de Géophysique Interne et Tectonophysique (UMR 5559), Grenoble, France

C. Darcel, P. Davy, and O. Bour
Géosciences Rennes (UMR6118), Rennes, France

Received 2 March 2001; revised 13 December 2001; accepted 18 December 2001; published 24 July 2002.

[1] In this paper, we characterize the geometry of damage zones that form around the main slip planes of normal faults. Specifically, we examine five faults of varying throws that affect the Nubian sandstones along the Suez rift. To quantify the density of cataclastic slip bands (CSBs) associated with the main slip plane, we recorded the position of all visible CSBs along a scan line perpendicular to the fault through to the damage zone. For each outcrop the scan line record is ~30 m long. Resulting density diagrams display concentrations of CSBs and clearly indicate a widening of the damage zone with increasing throw. A correlation integral was calculated for each CSB population in order to analyze both the scaling property of the density distribution and potential correlation lengths. From centimeter to meter scale, representing 2 orders of magnitude, the correlation integral appears adequately modeled by a power law, emphasizing the fractal property for the CSB distribution. For the five faults the calculated correlation dimension is constant within its error of determination, $D_c = 0.87 \pm 0.05$. The validity range of the fractal nature was derived from an adequate normalization of the correlation integral and from a comparison with synthetic fractal fracture networks. It appears that a finite correlation length corresponding to the damage zone width is detectable for meter-scale throws; for larger throws the correlation length is not detectable within the sampling domain. *INDEX TERMS:* 3250 Mathematical Geophysics: Fractals and multifractals; 8010 Structural Geology: Fractures and faults; 8109 Tectonophysics: Continental tectonics—extensional (0905); *KEYWORDS:* normal fault, damage zone, cataclastic slip band, correlation integral, Suez rift, Nubian sandstone

1. Introduction

[2] Many structural objects (fractures, veins, stylolites, etc.) constitute a zone of deformed rock around the main slip plane of a fault. This zone is defined as a "damage zone" [*Jamison and Stearns*, 1982; *Chester and Logan*, 1987; *McGrath and Davison*, 1995; *Beach et al.*, 1999] and is considered to be caused by fault propagation, linkage, or displacement along the fault [*Peacock et al.*, 2000]. Studying the structure of damage zones is important for understanding processes of fault growth, i.e., the modes of localization and propagation of rupture. An important application is to better constrain the geometry and evolution of fluid pathways around faults.

[3] Studies of the damage zone are thereby common and have often focused on the geometrical aspect of the zone by providing structural maps, detailed cross sections and microstructural analyses of deformation mechanisms [*Jamison and Stearns*, 1982; *Chester et al.*, 1993; *Antonellini and Aydin*, 1994; *McGrath and Davison*, 1995; *Schulz and Evans*, 1998]. For the typical case of porous sandstones the currently accepted model of the damage zone growth is based on the sequential development of cataclastic slip bands (CSBs) until the creation of a slip surface [*Aydin and Johnson*, 1978, 1983; *Underhill and Woodcock*, 1987], and it is supported by recent laboratory experiments [*Mair et al.*, 2000]. However, the field descriptions to date insufficiently describe the structure (size, organization) of the damage zone. Therefore more quantitative analyses were performed to define in particular the width of the damage zone in respect to the displacement [*Knott et al.*, 1996; *Beach et al.*, 1997, 1999; *Fossen and Hestammer*, 2000]. By calculating fracture density along scan lines perpendicular to fault strike, previous authors were able to define fractured zone within a background level. Microfracture density recorded at the thin section scale can also be used to determine the width of the damage zone [*Vermilye and Scholz*, 1998]. However, all the widths determined by density measurements are quite subjective and strongly depend on the chosen background level. Recently, on the basis of detailed maps of whole faults, *Shipton and Cowie* [2001] have presented a detailed three-dimensional (3-D) analysis focusing on the distribution of the CSB clusters to better characterize the internal structure of the damage zone and its growth processes. Here, by using the correlation

[1]Now at Department of Geological and Environmental Sciences, Stanford University, Stanford, California, USA.

0148-0227/02/2001JB000493$09.00

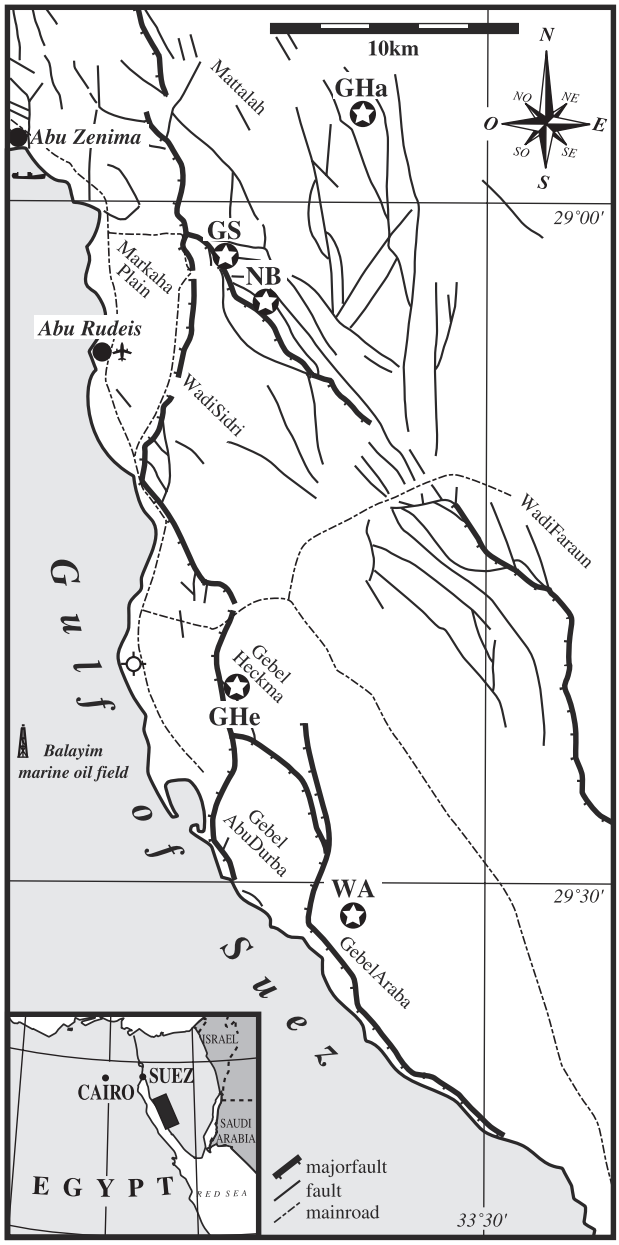

Figure 1. Simplified structural map of the study area located on the eastern border of the Suez rift (adapted from *Eyal et al.* [1980]). Stars indicate the location of the five studied faults affecting Nubian sandstones: Wadi Araba (WA, throw ~3 m), Gebel Hazbar (GHa, throw ~5 m), Naqb Budra (NB, throw ~30 m), Gebel Hekma (GHe, throw ~250 m), and Gebel Samra (GS, throw ~2500 m).

function we achieve a statistical analysis for characterizing first the spatial clustering of CSB populations and second the correlation length of the damage zone. Our approach is original in that we analyze the correlation properties of CSB distribution in the damage zone of faults with different degrees of maturity. By selecting five faults with meter- to kilometer-scale throws resulting from the same tectonic event, we can characterize the evolution of the fault structure and its heterogeneity with time.

[4] The correlation dimension was first used to quantify the "strangeness" of strange attractors in low-dimensional nonlinear systems exhibiting dynamical chaos [*Grassberger and Procaccia*, 1983] but has become popular in the analysis of laboratory acoustic emissions [*Hirata et al.*, 1987], earthquake epicenters [*Hirata*, 1989; *Hirata and Imoto*, 1991; *Öncel et al.*, 1996; *Eneva*, 1996] as well as fault scaling relationships [*Davy et al.*, 1990; *Gianquinta et al.*, 1999; *Bour and Davy*, 1999]. In this paper, we analyze the correlation properties of CSB positions recorded perpendicular to the damage zone trend. To assess the finite size effects of our natural data, we compare field data sets to synthetic fractal networks. Special attention is paid to scaling properties, which are the variation of CSB density with system scale and on the potential existence of a correlation length scale. The goal is to determine the width of the damage zone and how this width corresponds with throw and fault evolution. The five studied faults affect the Nubian sandstones of the Suez rift (Egypt). The study area, located on the western coast of the Sinai Peninsula (Figure 1), provides an ideal setting in which to study damage zone structure because of the remarkable outcrop quality and the extension-only tectonic history.

2. Geological Setting

2.1. Suez Rift and Nubian Sandstones

[5] The Gulf of Suez is an aborted arm of the Red Sea rift between the Sinai Peninsula and Africa (Figure 1). The Suez rift is a Neogene structure ~300 km long and 50–80 km wide that resulted from extension subperpendicular to the gulf borders [*Colletta et al.*, 1988]. Normal faults in the area mainly strike parallel to the rift axis at N140° (the "clysmic" direction defined by *Garfunkel and Bartov* [1977]) and define the boundaries of tilted blocks. Rifting began in early Miocene times (23.5 Ma) [*Chénet and Letouzey*, 1983; *Garfunkel and Bartov*, 1977] and essentially stopped with the transfer of the movement onto the Aqaba arm at the end of the Langhian (15 Ma) [*Ridcharson and Arthur*, 1988; *Steckler et al.*, 1988].

[6] The Nubian sandstones were deposited on a cratonic domain from the Cambrian to the end of the early Cretaceous and constitute the first deposits of the prerift sediments. This mainly sandy unit is up to 600 m thick and corresponds essentially to continental deposits [*Schütz*, 1994]. The prerift marine formations that cover the Nubian sandstones comprise a 500- to 1000-m-thick Cretaceous to Eocene succession of marine deposits that is subsequently overlain by conglomerate and evaporite synrift series in the center of the trough.

2.2. Normal Faults Studied

[7] The five normal faults studied, all resulting from the rifting process, are located on the western coast of the Sinai Peninsula between the cities of Abu Zenima to the north and El Tur to the south. In Figure 2 these faults are projected onto two schematic cross sections located in the northern and southern parts of the study area.

[8] To the north, the Gebel Samra fault has a throw of ~2.5 km, making it the largest structure studied. This fault represents the eastern border fault of the Suez rift. The Gebel Hazbar and Naqb Budra faults are located outside the rift at the east of the Gebel Samra fault and have throws of 5 and 30 m, respectively. To the south, the Wadi Araba fault is located in the Gebel Araba tilted block, which forms the

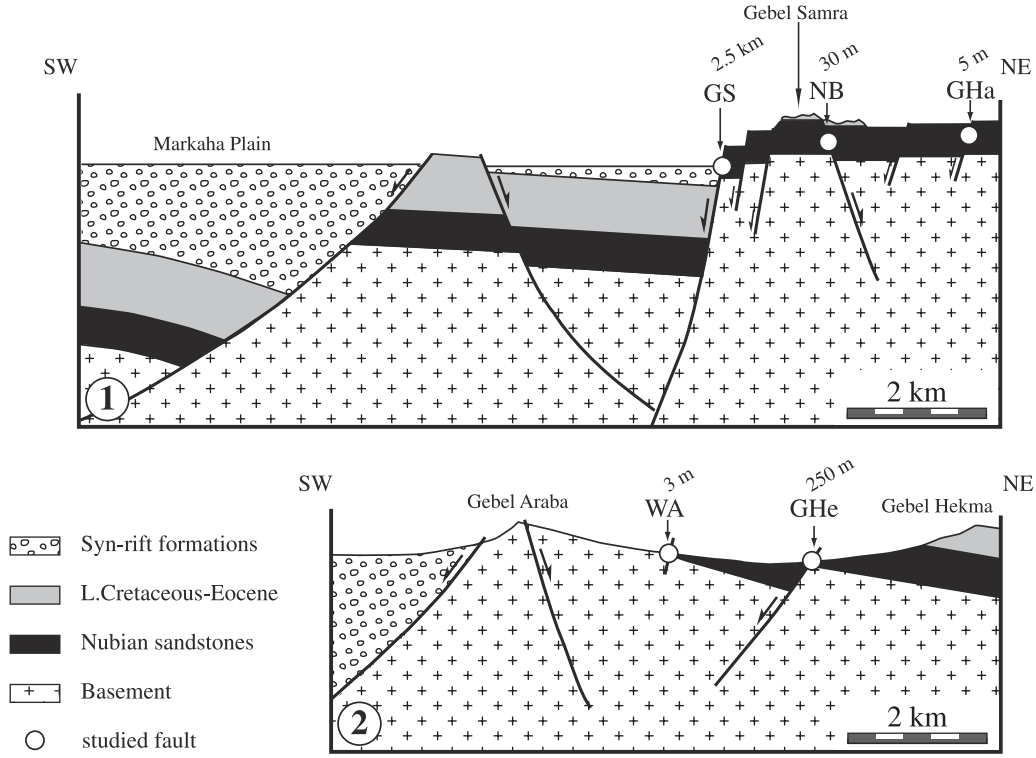

Figure 2. Schematic cross sections of the eastern Suez rift border (adapted from *McClay and Khalil* [1998] and *Colletta and Moretti* [1985]). Section 1 is located in the northern part of the study area (Figure 1) and section 2 is located in the southern part. This cartoon shows the structural location of the five faults of interest; GHa, Gebel Hazbar; NB, Naqb Budra; GS, Gebel Samra; GHe, Gebel Hekma; and WA, Wadi Araba.

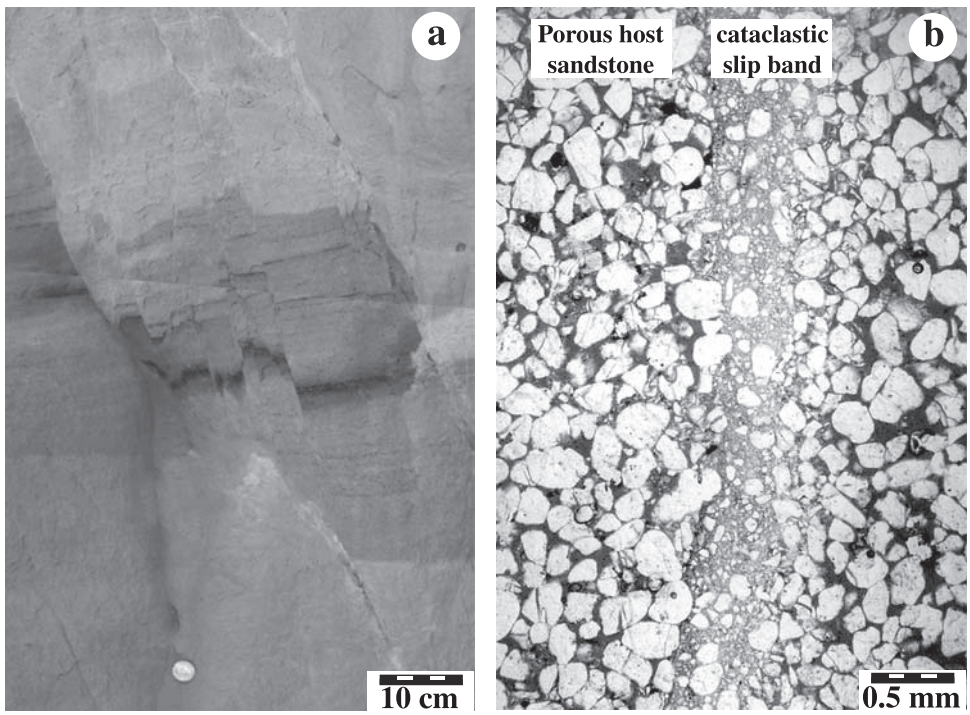

Figure 3. (a) Cataclastic slip bands in the Nubian sandstones observed in outcrop. The thin ferromagnesian stripes (dark) provide the offset marker (a few millimeters to decimeter) for each band. (b) Microstructure of a cataclastic slip band (thin section microphotograph). The quartz grains appear white and the injected epoxy resin filling pores is dark. In the cataclastic band the grain size and the porosity are drastically reduced compared to the host sandstone.

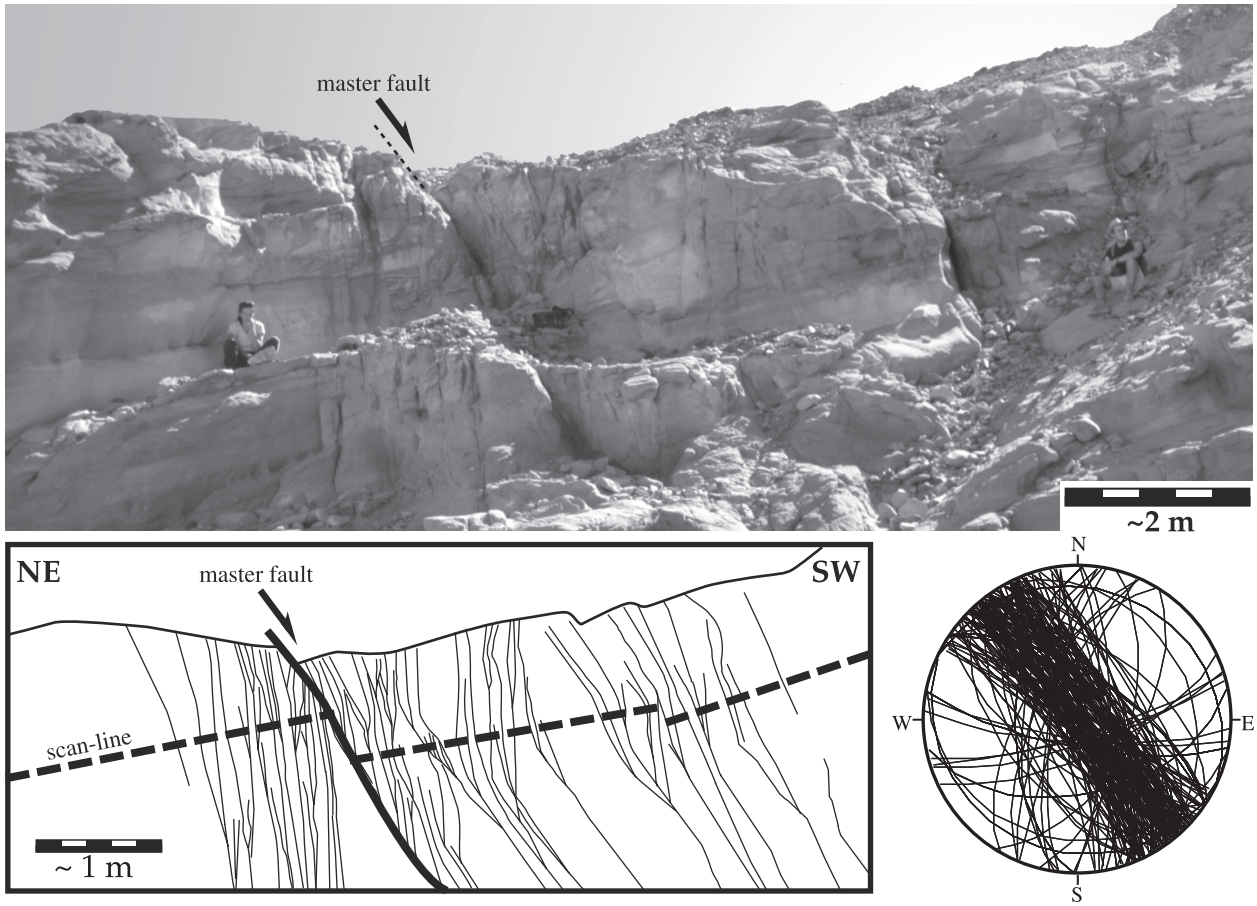

Figure 4. Studied outcrop of the Wadi Araba fault. The cartoon shows the main cataclastic slip bands qualitatively defining the damage zone around the master fault. The dashed line represents the scan line position used to record all visible CSBs. The Schmidt lower hemisphere stereogram shows that CSB strikes cluster round a main direction (N140°). The throw on the master fault is ∼80 cm, whereas the cumulated throw of the entire damage zone is ∼3.2 m.

footwall of the Araba Range fault. It is the smallest sampled structure, with a throw of ∼3 m. The Gebel Heckma fault has ∼250 m throw and is located in the footwall of a major normal fault situated to the north of the Wadi Araba block. All five faults are located at the border of the rift, i.e., in areas with little to no synrift deposition. Therefore we assume that burial of the Nubian sandstones in question did not exceed 1500 m, which corresponds to the maximum thickness of the overlying prerift series.

[9] We have analyzed deformation of the Nubian sandstones on both sides of the smaller offset Naqb Budra, Gebel Hazbar, and Wadi Araba faults. The Nubian sandstones outcrop only on the footwall side in the case of the two largest faults, Gebel Samra and Gebel Heckma. The exposure conditions of the selected faults are excellent. The damage zones are exposed with only limited gaps, and outcrop quality in the desert environment makes reliable observation of all macroscopic structures possible at an equivalent precision for all outcrops.

2.3. Deformation Markers in the Nubian Sandstones

[10] Shallow burial and limited diagenesis of the Nubian sandstones has resulted in a friable high-porosity material. Both optical and scanning electron (SEM) microscope observations of thin sections and sample fragments reveal weak meniscus cements of kaolinite, and our image analysis results indicate porosities of up to 20%. The deformation features are typical of porous sandstones consisting almost exclusively of cataclastic slip bands (CSBs) [*Antonellini et al.*, 1994; *Aydin and Johnson*, 1978; *Burhannudinnur and Morley*, 1997; *Fowles and Burley*, 1994; *Main et al.*, 2000; *Mair et al.*, 2000]. At the outcrop scale the CSBs appear as microfaults with a few millimeters to a decimeter of slip (Figure 3a). Microscopic observation indicates that CSBs are up to a few millimeters thick and are characterized by strong grain crushing and compaction (Figure 3b). Previous authors have shown that grain size reduction and compaction typically result in a significant drop in porosity and permeability within the CSB as compared to the host sandstone [*Antonellini and Aydin*, 1994; *Fowles and Burley*, 1994; *Underhill and Woodcock*, 1987] (Figure 3b). Crushing, compaction, and consolidation render the CSBs more resistant to weathering than the host rock, which also makes them relatively easy to identify and examine in exhaustive detail. Because of their subvertical dip, the possibility remains that some of the CSBs may have evolved from preliminary joints form in sheared zones.

[11] All the CSBs macroscopically associated to the main slip plane qualitatively define the damage zone (Figure 4). Damage zones in the Nubian sandstones range from a few

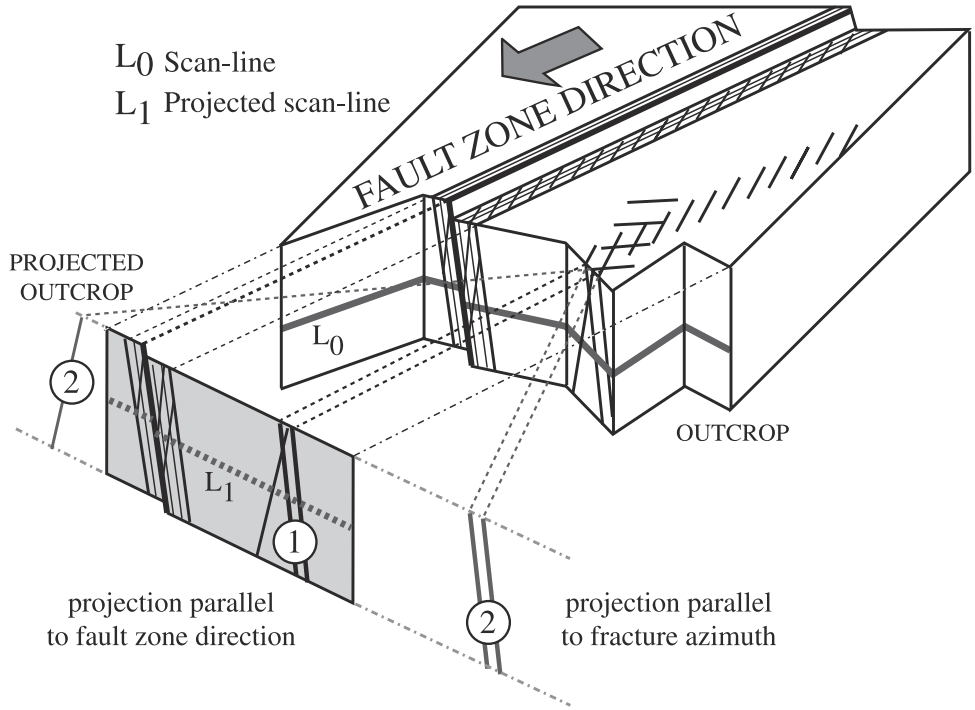

Figure 5. Cartoon showing the method of data collection used in this study. To measure CSB positions, the transverse scan line L_0 is located on an irregular vertical section. Positions are then projected onto an "ideal" scan line L_1 perpendicular to the fault zone in order to obtain real distances between CSBs. To preserve cluster organization, each CSB is projected parallel to fault zone direction (1). Note that projection parallel to the CSB azimuth destroys the clusters (2).

meters to a few hundreds of meters wide [*Beach et al.*, 1999]. In the case of the Wadi Araba, Gebel Hazbar, Gebel Heckma, and Gebel Samra faults, Schmidt lower hemisphere stereogram representations show that CSB strikes cluster around a main direction at N140° (Figure 4), suggesting that the faults are planar in structure. The damage zone at Naqb Budra features two associated CSBs sets with different average strikes (N030° and N155°).

[12] Fault offset is primarily concentrated along one or two slip planes, but some slip is also distributed among the surrounding CSBs. In the Wadi Araba damage zone the occurrence of prefaulting sedimentary markers (paleosol ferruginous bands) allows for an accurate determination of the offset accommodated by each CSB. The throw on the master fault is ~80 cm, whereas all throws are millimeter to centimeter scale on the other CSBs. By summing the throws measured on each CSB the cumulative throw across the entire damage zone is ~3.2 m. Because of the massive nature of sandstone bedding adjacent to the other four faults, precise offset determinations are rarely possible in these cases. Nevertheless, general bed geometry constraints indicate that most CSB offsets outside the master fault are less than a few tens of centimeters. Thus the total throw across these damage zones is estimated to approximately equal that on the major faults.

3. CSB Density in the Damage Zone

3.1. Field Data Acquisition

[13] To characterize the deformation distribution in each damage zone, we systematically plotted the CSBs cut by a scan line across the fault. The scan line was located on a vertical, bedding-normal outcrop, and within a single sand layer so as to negate the possible effects of petrophysical differences. We recorded the position, azimuth, and dip of each CSB, as well as the throw and thickness when possible.

[14] Because of outcrop topography, each scan line is composed of several rectilinear segments of different orientation. Therefore CSB positions had to be projected onto an "ideal" scan line oriented perpendicular to the fault zone trend to obtain the real distances between CSBs (Figure 5). Qualitative structural analysis suggests that CSBs tend to form genetically related, geometrically connected clusters of finite length. Therefore the mode of projection must preserve the cluster organization. If each CSB were projected parallel to its azimuth, the cluster organization would be destroyed because all recorded CSBs are not parallel. Therefore we have chosen to project CSB position parallel to the average azimuth of the damage zone, as determined on bedding surfaces observed close to the scan line.

[15] Although all recorded positions are given with centimeter-scale precision, the lower limit of CSB position resolution at all five faults is estimated to ~5 cm because of difficulties in adjusting the tape measure parallel to the measured bed and between the individual measured segments. The outcrop conditions being identical for the five faults, the lower limit of resolution is thus the same for all measured populations.

3.2. Description of the CSB Density Around the Main Faults

[16] For each fault the CSB density is defined as the number of CSBs per meter in 0.2-m-long bins plotted as a function of distance (Figure 6.). On each diagram the master

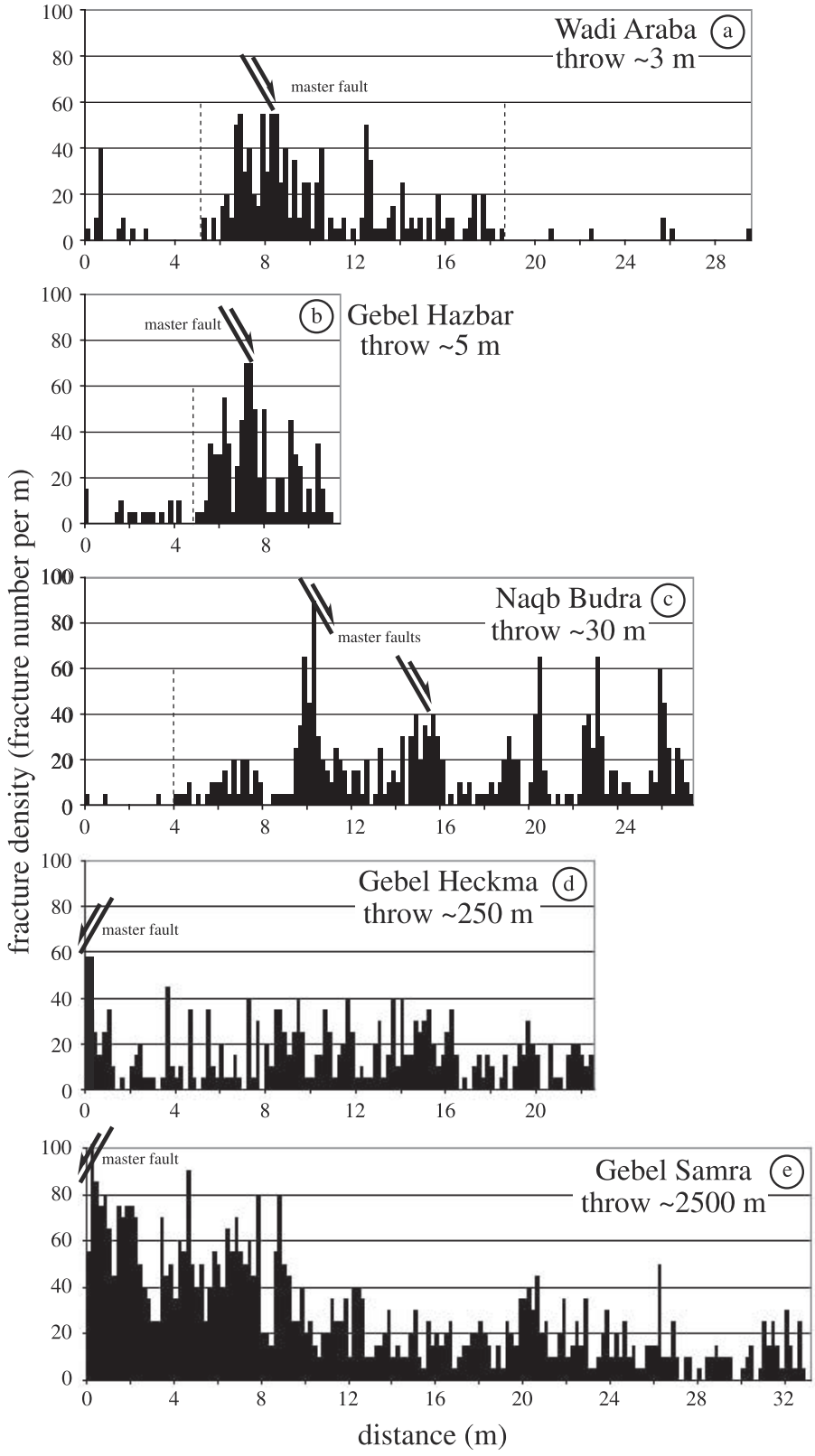

Figure 6. Diagrams of CSB density for natural data sets of the five studied faults. Density is defined as the number of CSBs per meter within each 0.2-m-wide segment. Vertical dashed lines indicate the limit of damage zones qualitatively defined as five CSBs per meter. For meter- to decameter-scale throws (Figures 6a–6c), CSB clusters are well defined, whereas for larger throws (Figures 6d and 6e) the CSB density increases between clusters.

fault position and the slip direction are indicated. These density diagrams illustrate three important features:

1. Damage zones of faults with throw of less than a few tens of meters (Wadi Araba, Gebel Hazbar, and Naqb Budra) show high CSB concentrations (60–80 CSBs per meter) in well-defined clusters up to a few meters wide. For faults with hectometer- to kilometer-scale throw (Gebel Heckma and Gebel Samra), some peaks of density are visible but are much less individualized than for smaller throws. In fact, the peak values are similar to those in the small throw fault zones; that is, the apparently weaker clustering is due to the higher CSB density between clusters with larger throw.

2. CSB density decreases with distance from the master fault. However, because of the cluster existence, this decrease is irregular. For faults of small throw, CSB density drops off to background levels (qualitatively defined as five CSBs per meter) a few meters away from the master fault, thus defining the boundaries of the damage zone. For the Wadi Araba fault the width of the damage zone is 13 m (3.5 m in the footwall and 9.5 m in the hanging wall). For the Gebel Hazbar and Naqb Budra faults the footwall damage zone widths are 2.5 and 6 m, respectively. The hanging wall damage zone widths for these two faults exceed the scan line lengths: 4 m for the Gebel Hazbar fault and 18 m for the Naqb Budra fault. At Naqb Budra, both observed CSB sets show an increase in CSB density with proximity to the master faults, indicating that both sets are genetically related to fault activity. For the Gebel Heckma and Gebel Samra faults the Nubian sandstones are visible only in the footwall side, where the damage zone width exceeds the scan line length of 22 and 32 m, respectively. It is worth noting that outcrops located outside the observation area gaps suggest that the damage zone exceeds 32 m in width for the Naqb Budra fault hanging wall and 70 m in width for the Gebel Samra fault footwall.

3. Where both sides of the faults were analyzed, the hanging wall displays both a higher CSB density and a wider damage zone than the footwall. This density asymmetry supports previous analysis regarding fracture frequency in normal fault damage zones affecting Nubian sandstones [*Knott et al.*, 1996].

4. Correlation Analysis

4.1. Correlation Integral Scaling

[17] Numerous studies have investigated the fractal nature of the fracture networks by using different methods for measuring the fractal dimension [*Bonnet et al.*, 2001]. In the particular case of the one-dimensional (1-D) analysis, several studies characterized the spatial distribution of fractures through a ''spacing distribution'' or ''interval counting'' (a 1-D application of the 2-D ''box counting'') [*Brooks and Allmendiger*, 1996; *Gillespie et al.*, 1993; *Needham et al.*, 1996]. Actually, if the box-counting method is adapted for determinist fractal networks as Cantor dust or Von Koch curve, it can become a troublesome procedure when it is applied for statistical fractal networks [*Vicsek*, 1989]. For a natural system the most efficient method for measuring scaling properties consists of calculating the correlation integral, which applies to a set of points [*Vicsek*, 1989]. By measuring the distances between each individual fracture and all the others, correlation analysis is robust with regard to the fracture density and describes precisely the distribution of fractures densities. Similar analyses in two dimensions have already achieved excellent results to describe the spatial distribution of fracture center points [*Davy et al.*, 1990; *Bour*, 1997; *Bour and Davy*, 1999; *Gianquinta et al.*, 1999].

[18] To calculate the correlation integral, we use the discretized equation of *Grassberger and Procaccia* [1983], adapted as

$$C\left(\frac{r}{L}\right) = \frac{2}{N(N-1)L}\left(\sum_{i<j}\Theta\left(r-\left|x_i-x_j\right|\right)\right) \approx \left(\frac{r}{L}\right)^{D_c}, \quad (1)$$

where r is a distance, N is the total number of CSBs, L is the scan line length, x is the CSB position, and Θ is the Heaviside function (defined as $\Theta(X) = 1$ if $X > 0$ and $\Theta(X) = 0$ if $X < 0$). The correlation function measures the number of pairs of CSBs whose distances apart ($x_i - x_j$) is less than distance r. By varying r, we can plot in a logarithmic diagram the correlation integral versus the distance. The slope of the correlation integral line calculated by a linear regression gives the exponent D_c of the power law. For a linear distribution (1-D analysis), D_c varies from 1 (for CSBs homogeneously distributed along the scan line) to 0 (for CSBs localized at a single point). To check the validity of the power law model, we calculate and plot the local logarithmic slope ($d \ln C(r)/d \ln r$), which is theoretically varying around the fractal dimension in the perfect fractal model.

[19] The normalization by $N(N\text{-}1)$ and L makes the correlation integral independent of the system size (this is obvious for $r = L$ since $C(1) = 1$ whatever the value of L) and thus makes possible the comparison of different CSB populations. Characterizing the correlation degree allows us to distinguish a well-correlated synthetic population such as the Cantor dust $D_c = 0.63 \pm 0.02$ (theoretically, $D_c = \ln 2/\ln 3 = 0.63$) from an uncorrelated synthetic population such as a random population $D_c = 0.99 \pm 0.01$ (theoretically, $D_c = 1$) (Figure 7).

4.2. Spatial Distribution of CSBs

[20] Figure 8 shows the correlation integral and local slope curves for the five faults studied. The data are compared to an average of 1000 synthetic realizations similar to this shown in Figure 9, which is conditioned to have the same statistical properties as the real data set by using a fractal generator [*Darcel et al.*, 2000]. Note that the synthetic data are considerably smoothed by the reductions in statistical fluctuation by averaging over a large number of realizations. Normalization (equation (1)) by the number of CSBs (N) and the scan line length (L) allows us to compare directly all the different CSB populations.

[21] Within statistical fluctuations the local slope is constant over the scale range 10^{-3}–10^{-1} units on Figure 8, at the exception of the Naqb Budra CSB population. These 2 orders of magnitude demonstrate that natural CSB distributions can undoubtedly be described with a power law. A scale range of just 1 order could not exclude other possible distributions such as exponential or lognormal (see discussion by *Bonnet et al.* [2001]). The correlation dimension is calculated by a regression of the integral within the part delimited by the local slope plateau. This bounded domain defines the scaling interval of validity where the correlation dimension calculated for natural data sets can be applied

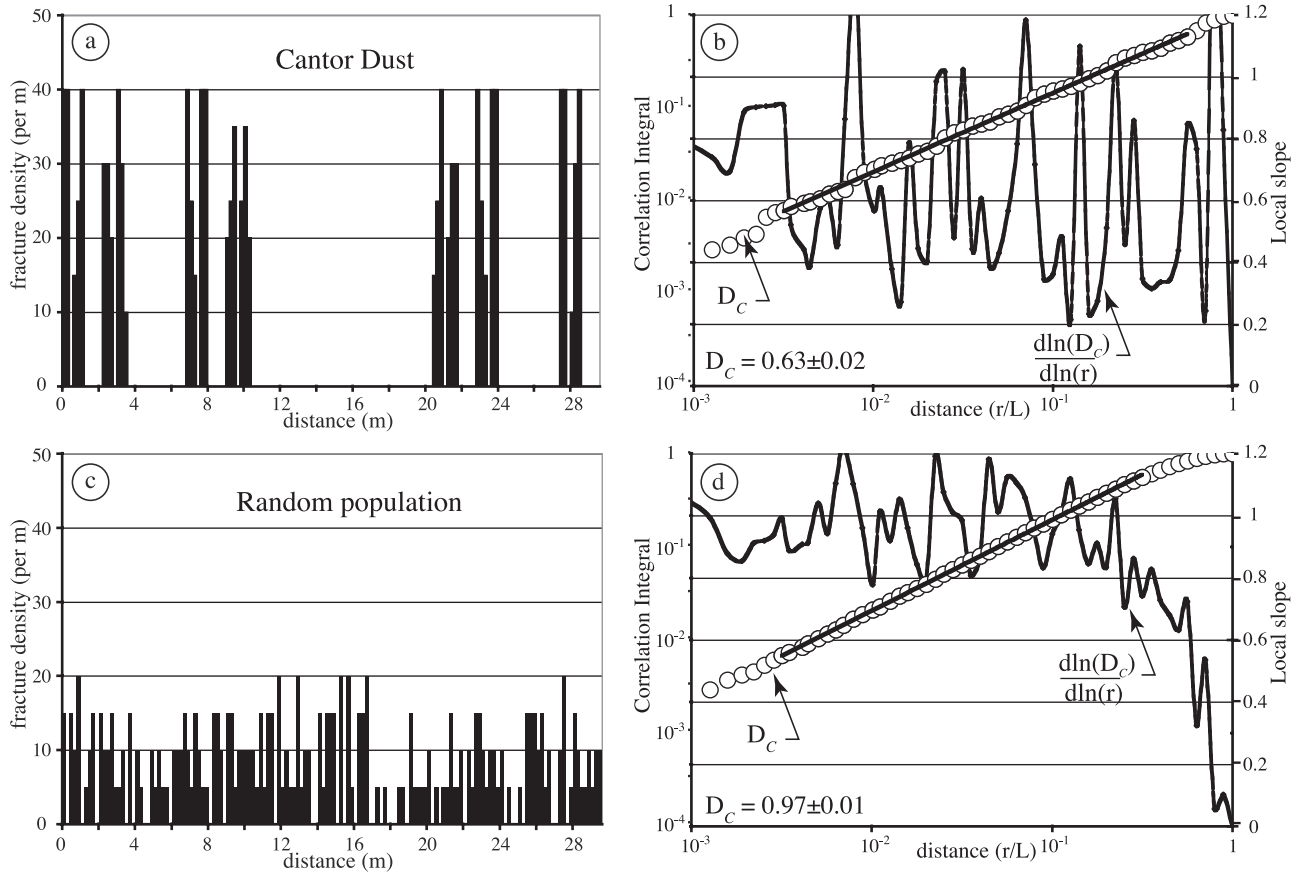

Figure 7. Diagrams of CSB density and calculation of correlation integral for synthetic data sets. These synthetic populations are generated with the same features as the Wadi Araba fault, i.e., scan line length of 30 m and CSB number of 236. (a) Cantor dust case. CSB density shows several clusters. (b) Calculated D_c of 0.63 ± 0.02. The high fluctuations of the associated local slope are due to the specific making process of this determinist population. (c) Random population. CSBs are homogeneously distributed, and the CSB density does not show cluster. (d) Calculated D_c of 0.99 ± 0.01, close to the theoretical value of 1.

and corresponds to the fractal bandwidth defined by *Bonnet et al.* [2001]. The correlation dimension value for each fault is presented in Table 1.

[22] The error of determination cannot be calculated lower than 0.05. First, the limits of the bandwidth where the correlation integral can be calculated are not obvious, and their determination has a slight influence on the correlation dimension. Second, natural systems are not supposed to be exact deterministic fractal. They do have a stochastic component that comes from the fracturing process, which introduces some intrinsic variability around any geometrical model of natural data. By comparison with results from a stochastic fractal generator, we estimate the average uncertainty on the fractal dimension to be ~0.05 owing to this stochastic component and to finite size effects. As a consequence, the correlation dimension calculated for the five faults is constant within its error of determination, $D_c = 0.87 \pm 0.05$.

[23] In the case of the Naqb Budra CSB population (Figure 8c), a short plateau of the local slope spanning just less than 1 order of magnitude for the small scales is identifiable yielding a $D_c = 0.88 \pm 0.05$. This lack of a wide plateau may be explained either by the mechanical interaction of the two CSB sets or as an artifact of the projection method used to average the azimuth direction. However, when the correlation integral technique is applied separately to both CSB sets, the local slope of each CSB set remains the same as for the total data set, i.e., without displaying a clear long plateau.

4.3. Correlation Length Scale

[24] On Figure 8 the fit between the natural and generated correlation integral curves is excellent for faults with large throw (Naqb Budra, Gebel Heckma, and Gebel Samra). For the two smallest faults with meter-scale throw (Wadi Araba and Gebel Hazbar), although the slopes of integral straight line are the same, the synthetic correlation integral curves are systematically offset from the data. Knowing that the two populations have the same D_c and the same parameters (scan line length and number of CSBs), the shift represents the existence of a correlation length scale (ξ) as shown by the following derivation. The correlation length represents the scale where CSBs are spatially correlated, and thereby it may differ from the damage zone width that corresponds to all CSBs genetically related to the fault.

[25] Assuming the length of the scan line (L) is larger than the correlation length scale (ξ) and correlation length

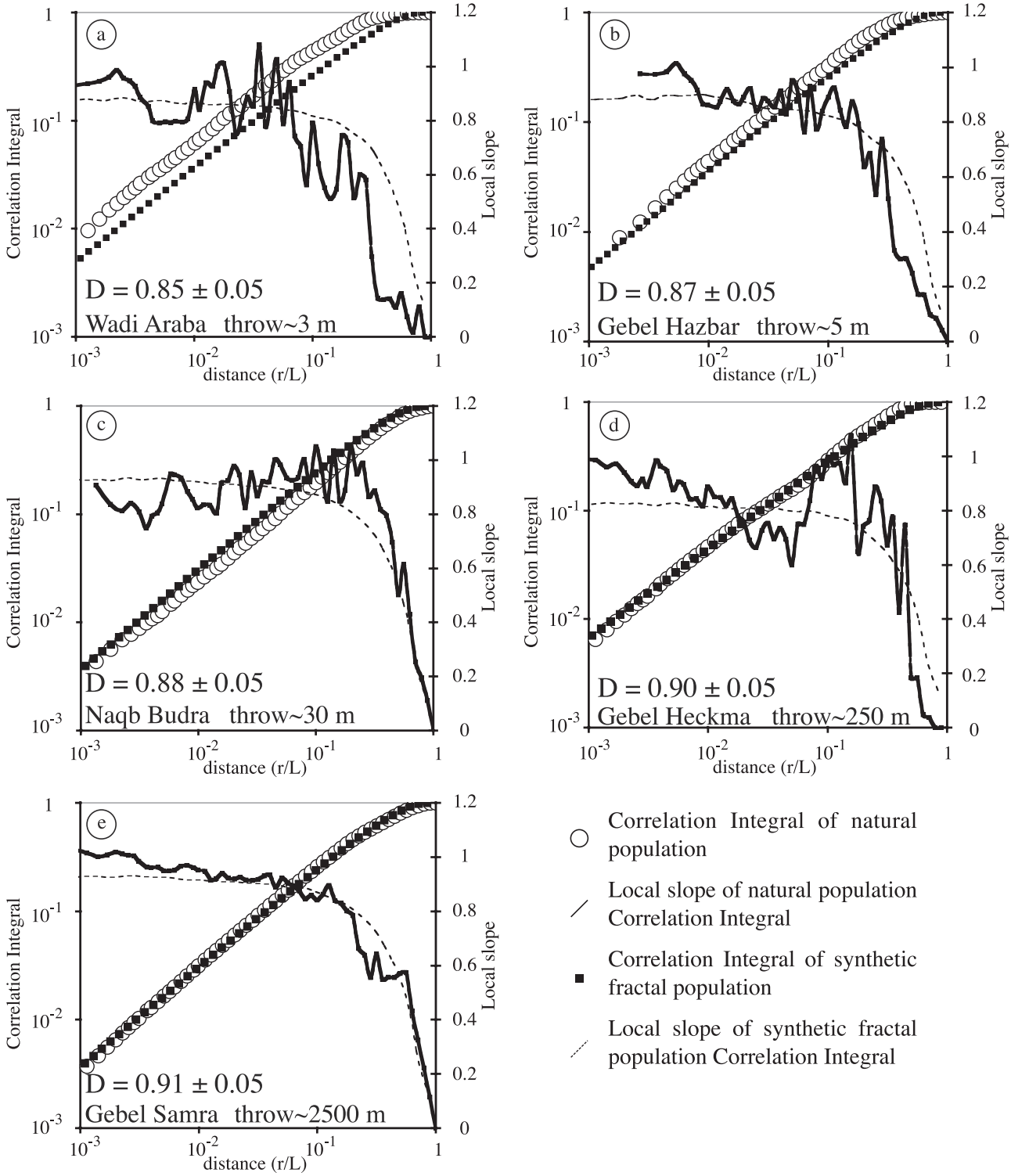

Figure 8. Comparison of correlation integral diagrams of natural data and generated data for the five studied faults. Circles correspond to the correlation integral of natural population, and the solid line corresponds to the associated local slope. Squares represent the correlation integral of the generated population, and the dashed line represents the associated local slope. For each fault, averaging 1000 drawings using the same input parameters smoothes the local slope curve, reducing noise and emphasizing the plateau. Fit between both populations is excellent for hectometer- and kilometer-scale throws. For meter-scale throws, however, the natural distribution is shifted on the small-scale side.

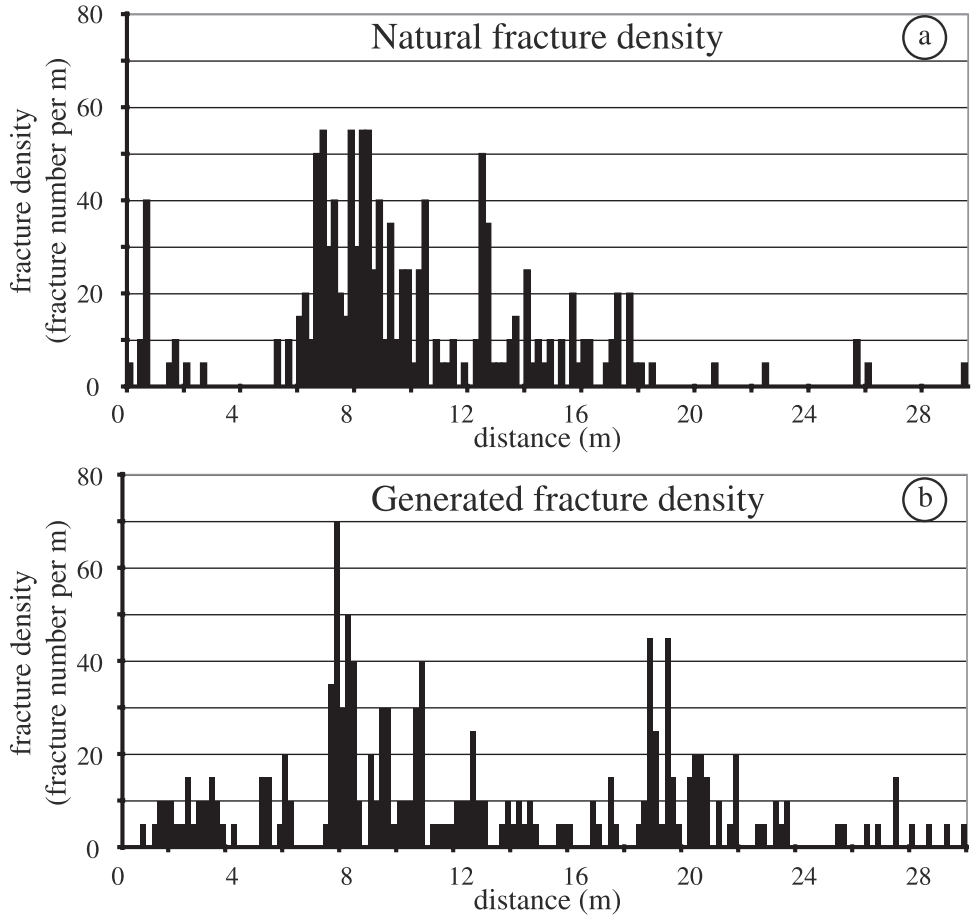

Figure 9. (a) Comparison of CSB density diagrams of the natural population of the Wadi Araba fault and (b) one example of corresponding generated populations having the same scan line length, CSB number, and D_c. CSB distributions show clusters in both cases. Nevertheless, CSB clusters appear clearly focused around the main slip plane for the natural distribution, whereas they are scattered along the scan line for generated data.

scale is the width of the damage zone, we know that the correlation integral is given by

$$C(r) \approx \left(\frac{r}{\xi}\right)^{D_c} \qquad L > \xi.$$

[26] We can then introduce L by writing

$$C(r) = \left(\frac{r}{L}\right)^{D_c}\left(\frac{L}{\xi}\right)^{D_c} \qquad L > \xi.$$

[27] In this case, $(L/\xi)^{D_c}$ represents the value of the shift between the correlation integrals of the natural CSB population and the model. Then ξ can be calculated by using the y intercept in a log-log diagram where the equation represents a line

$$\underbrace{\log C(r)}_{Y} = \underbrace{D_c \log\left(\frac{r}{L}\right)}_{D_c X} + \underbrace{D_c \log\left(\frac{L}{\xi}\right)}_{A}$$

Thus ξ is obtained from $\xi = L\ 10^{-A/D_c}$ where A is the y intercept of the model population in the logarithmic diagram.

[28] For the Wadi Araba fault the calculated correlation length scale is equal to 15 m. This value is close to the 13 m width of the damage zone defined from the density diagram (Figure 6a). In the Gebel Hazbar case the calculated correlation length scale is equal to 8.5 m. This value is close to the 6 m width of the CSB concentration around the master fault (Figure 6b). However, this may be an underestimate, since the hanging wall was incompletely sampled.

[29] This analysis allows us to determine the boundaries of the population of spatially correlated CSBs, which

Table 1. Fault Data

	Wadi Araba	Gebel Hazbar	Naqb Budra	Gebel Hekma	Gebel Samra
Estimated throw, m	3	5	30	250	2500
Damage zone,[a] m	15	$\geq$ 8.5	>46	>22	>70
Scan line length,[b] m	30	12	28	22	33
CSB number[b]	236	173	360	344	925
Calculated D_c	0.85	0.87	0.88	0.90	0.91

[a] At Naqb Budra and Gebel Samra, values include outcrop segments located beyond observation gaps and not sampled for statistical analyze.

[b] Scan line length and cataclastic slip band (CSB) numbers are those used for statistical analysis and correspond to continuous outcrop intervals around the master fault(s).

coincide with those of the qualitatively defined damage zones for the small faults. Because we were unable to completely sample the influence zone of larger throw faults, we could not calculate correlation length scales for them. In particular, we could not study the hanging wall of faults with kilometer-scale throw. Nevertheless, we can propose a lower bound of the correlation length scale that is at least greater than the scan line length. With this consideration, it appears that the correlation length increases from faults with meter-scale throw to larger faults.

5. Discussion

[30] We consider the five studied faults as representative of different steps within a progressive damage zone formation process. This assumption is realistic because all the faults result from the same extensional tectonic event affecting the same lithology with similar burial histories. The conditions and the mechanisms of deformation are thus equivalent. Nevertheless, we cannot ignore the potential effects of varying rheological properties across the fault as offset progresses.

[31] First, our results indicate that the correlation dimension is independent of fault throw; that is, the correlation dimension is constant for the five faults within the error of measurement. Therefore the scaling properties of CSB distributions that remain identical during the fault growth can be considered as scale-invariant. Nevertheless, the scaling properties are limited up to the width of the damage zone, which plays the role of a correlation length. With our data collection we can calculate a correlation length, which is equal to the damage zone width for the small faults. Our approach differs from that of *Beach et al.* [1999], who arbitrarily define the damage zone as having a frequency greater than five CSBs per 0.5 m. On the other hand, we can just assume that this length is at least greater than scan line length for the largest faults. From this, we conclude than the correlation length scales are greater for faults with decameter- to kilometer-scale throw than for faults with meter-scale throw, but we are unable to precisely constrain this increase with our data. In particular, we cannot establish that the correlation length scale remains equal to the damage zone width. Moreover, by only considering the location of CSBs, the results regarding correlation properties are established for the finite deformation within the damage zone and do not take in account the active substructure. For a better understanding of strain localization during fault development it would be necessary to improve data collection by systematically recording additional information such as individual CSB throw.

[32] Second, our results show that increased throw induces an increase of finite deformation. On the basis of the qualitative results of the CSB density diagrams, fault damage zone width increases systematically with increasing throw. Moreover, CSB density increases between CSB clusters as throw increases. Thus throw appears to be a control on the growth of a damage zone. However, our conclusions are well controlled only for faults with small (up to decameter-scale) throws for which we could observe the whole damage zone, and owing to the limited extent of our scan lines, they remain speculative for those with larger throw. The widening of the damage zone with increasing throw matches the observations of *Beach et al.* [1999], but we cannot confirm the damage zone width limit of ~100 m observed by them for the largest throws.

[33] Our results and those of *Beach et al.* [1997, 1999] and *Shipton and Cowie* [2001] suggest that the damage zone widens with increasing the throw on the master fault. Moreover, the density of the whole damage zone calculated as the ratio of the number of CSBs to the characteristic length (damage zone width for the small faults or scan line length for the larger faults) is almost the same for the five faults. Therefore, even after a throughgoing slip surface develops, the subsequent deformation is accommodated along new CSBs within the damage zone as well as by slip on the master fault. These results do not totally fit with the currently accepted model for porous sandstones that considers the creation of the slip surface as the last step of the fault zone development [*Aydin and Johnson*, 1978]. According to our analysis the increase of both damage zone width and CSB density continues after the slip surface formation. The fact that deformation is not totally localized on this discrete surface can be related to the rotations and geometrical effects such as those described in faulted sandstones by *Davis et al.* [2000] and *Steen and Andresen* [1999].

6. Conclusions

[34] This study of CSB distribution in the damage zones of faults affecting the Nubian sandstones of the Suez rift demonstrates that scaling properties do not depend on fault throw but correlation length and damage zone width increase with throw. On the basis of our 1-D quantitative field analysis, the main results can be summarized as follows:

1. CSB density diagrams allow us to qualitatively define fault damage zones from the concentration of CSBs around the main slip planes. According to these diagrams, CSB density decreases irregularly with increasing distance from the master fault, and the damage zone widens with increasing throw. Qualitatively, CSB density increases between CSB clusters as the throw increases; thus density peaks appear less individualized for faults with larger throws.

2. The correlation integral analysis can be used to characterize the degree of organization of CSBs within damage zones. CSB distribution can be described by a power law: $C(r) \sim ar^{D_c}$. For the damage zones examined here, D_c lies in the range $D_c = 0.87 \pm 0.05$ and therefore does not vary significantly with throw. Finite size effects can be identified by comparing natural data with synthetic fractal networks. From this, the predictive distribution can be applied from centimeter to meter scales.

3. The existence of a correlation length scale (ξ) for faults of meter-scale throw has been demonstrated. The correlation length corresponds to the damage zone width. To our knowledge, it is the first time that a correlation length scale has been defined for a CSB distribution. Where unobstructed scan line reaches to the boundaries of the damage zone, we can calculate a correlation length. Where it does not, typically for larger throw, we can only estimate a lower bound for the correlation length. The correlation length scale increases from faults with meter-scale throw to faults with larger throw.

[35] **Acknowledgments.** This research was supported by IFP through a convention with LGIT, Joseph Fourier University (Grenoble). P. Davy, C. Darcel, and O. Bour received financial support from the European Community (contract SALTRANS EVKI-CT-2000-00062). We are grateful to I. Moretti and B. Colletta for their confidence and their help in the field. We thank J.F. Gamond, F. Lahaie, and J.R. Grasso for critical discussions and comments on these results. We would like to thank the two reviewers, Z. Shipton and G. Yielding, for their helpful comments. Thanks are also owed to the Associate Editor, I. Main, whose constructive review and insightful suggestions have greatly improved the second draft of the manuscript.

References

Antonellini, M., and A. Aydin, Effect of faulting on fluid flow in porous sandstones: petrophysical properties, *AAPG Bull.*, *78*(3), 355–377, 1994.

Antonellini, M., A. Aydin, and D. Pollard, Microstructure of deformation bands in porous sandstones at Arches National Park, Utah, *J. Struct. Geol.*, *16*, 941–959, 1994.

Aydin, A., and A. M. Johnson, Development of fault as zone deformation bands and as slip surfaces in sandstone, *Pure Appl. Geophys.*, *116*, 922–929, 1978.

Aydin, A., and A. M. Johnson, Analysis of faulting in porous sandstones, *J. Struct. Geol.*, *5*, 19–31, 1983.

Beach, A., J. L. Brown, A. I. Welbon, J. E. McCallum, P. J. Brockbank, and S. D. Knott, Characteristics of fault zones in sandstones from NW England: Application to fault transmissibility, in *Petroleum Geology of the Irish Sea and Adjacent Areas*, edited by N. S. Meadows et al., *Geol. Soc. Spec. Publ.*, *124*, 185–194, 1997.

Beach, A., A. I. Welbon, P. J. Brockbank, and J. E. McCallum, Reservoir damage around faults: Outcrop examples from Suez rift, *Pet. Geosci.*, *5*, 109–116, 1999.

Bonnet, E., O. Bour, N. E. Olding, P. Davy, I. Main, P. A. Cowie, and B. Berkowitz, Scaling of fracture systems in geological media, *Rev. Geophys.*, *39*(3), 347–383, 2001.

Bour, O., Transferts de fluides dans les milieux fracturés—Effets d'Echelle, *Mém. 80*, Geosci. Rennes, Rennes, France, 1997.

Bour, O., and P. Davy, Clustering and size distributions of fault pattern: Theory and measurements, *Geophy. Res. Lett.*, *26*(13), 2001–2004, 1999.

Brooks, A. B., and R. W. Allmendiger, Fault spacing in the El Teniente Mine, central Chile: Evidence for nonfractal geometry, *J. Geophys. Res.*, *101*, 13,633–13,653, 1996.

Burhannudinnur, M., and C. K. Morley, Anatomy of growth fault zones in poorly lithified sandstones and shales: Implications for reservoir studies and seismic interpretation, part 2, Seismic reflection geometries, *Pet. Geosci.*, *3*, 225–231, 1997.

Chénet, P. Y., and J. Letouzey, Tectonique de la zone comprise entre Abu Durba et Gebel Mezzazat (Sinaï, Egypte) dans le contexte de l'évolution du Rift de Suez, *Bull. Cent. Rech. Explor. Prod. Elf-Aquitaine*, *7*(1), 201–215, 1983.

Chester, F. M., and J. M. Logan, Composite planar fabric of gouge from the Punchbowl Fault, California, *J. Struct. Geol.*, *9*, 621–634, 1987.

Chester, F. M., J. P. Evans, and R. L. Biegel, Internal structure and weakening mechanisms of the San Andreas Fault, *J. Geophys. Res.*, *98*, 771–786, 1993.

Colletta, B., and I. Moretti, Analyse structurale dans la région de Wadi Baba (Rift du golfe de Suez), report, Inst. Fr. du Pét., Rueil-Malmaison, France, 1985.

Colletta, B., P. Le Guellec, J. Letouzey, and I. Moretti, Longitudinal evolution of the Suez rift structure (Egypt), *Tectonophysics*, *153*, 221–233, 1988.

Darcel, C., O. Bour, P. Davy, and J. R. de Dreuzy, A discrete geometrical model of fractured media for stochastic fluid flow simulation, paper presented at XXV General Assembly, Eur. Geophys. Soc., Nice, France, 2000.

Davis, G. H., A. P. Bump, P. E. Garcia, and S. G. Ahlgren, Conjugate Riedel deformation band, shear zones, *J. Struct. Geol.*, *22*, 169–190, 2000.

Davy, P., A. Sornette, and D. Sornette, Some consequences of a proposed fractal nature of continental faulting, *Nature*, *348*, 56–58, 1990.

Eneva, M., Effect of limited data sets evaluating the scaling properties of spacially distributed data: An example from mining-induced seismic activity, *Geophys. J. Int.*, *124*, 773–786, 1996.

Eyal, M., Y. Bartov, A. E. Shimron and Y. K. Bentor, Sinai—Geological map, scale 1:500,000, Surv. of Isr., Jerusalem, 1980.

Fossen, H., and J. Hestammer, Possible absence of small faults in the Gulfaks Field, northern North Sea: Implications for downscaling of faults in some porous sandstones, *J. Struct. Geol.*, *22*, 851–863, 2000.

Fowles, J., and S. Burley, Textural and permeability characteristics of faulted, high porosity sandstones, *Mar. Pet. Geol.*, *11*, 608–623, 1994.

Garfunkel, Z., and Y. Bartov, The tectonics of Suez rift, *Bull. Geol. Surv.*, *71*, 1977.

Gianquinta, A., S. Boccaletti, M. Boccaletti, and L. Piccardi, Investigating the fractal properties of geological fault systems: The main Ethiopian rift case, *Geophys. Res. Lett.*, *26*(11), 1633–1636, 1999.

Gillespie, P. A., C. B. Howard, W. J. J., and J. Watterson, Measurement and charaterisation of spatial distributions of fractures, *Tectonophysics*, *226*, 113–141, 1993.

Grassberger, P., and I. Procaccia, Measuring the strangeness of strange attractors, *Physica D*, *9*, 189–208, 1983.

Hirata, T., A correlation between the *b* value and the fractal dimension of earthquakes, *J. Geophys. Res.*, *94*, 7507–7514, 1989.

Hirata, T., and M. Imoto, Multifractal analysis of spatial distribution of microearthquakes in the Kanto region, *Geophys. J. Int.*, *107*, 155–162, 1991.

Hirata, T., T. Satoh, and K. Ito, Fractal structure of spatial-distribution of microfracturing in rock, *Geophys. J. R. Astron. Soc.*, *90*, 369–374, 1987.

Jamison, W. R., and D. W. Stearns, Tectonic deformation of Wingate Sandstone, Colorado National Monument, *AAPG Bull.*, *66*(12), 2584–2608, 1982.

Knott, S. D., A. Beach, P. J. Brockbank, J. L. Brown, J. E. McCallum, and A. I. Welbon, Spatial and mechanical controls on normal fault populations, *J. Struct. Geol.*, *18*, 359–372, 1996.

Main, I., O. Kwon, B. T. Ngwenya, and S. C. Elphick, Fault sealing during deformation-band growth in porous sandstone, *Geology*, *28*, 1131–1134, 2000.

Mair, K., I. Main, and S. Elphick, Sequential growth of deformation bands in the laboratory, *J. Struct. Geol.*, *22*, 25–42, 2000.

McClay, K., and S. Khalil, Extensional hard linkages, eastern Gulf of Suez, Egypt, *Geology*, *26*, 563–566, 1998.

McGrath, A. G., and I. Davison, Damage zone geometry around fault tips, *J. Struct. Geol.*, *17*, 1011–1024, 1995.

Needham, T., G. Yielding, and R. Fox, Fault population description and prediction using examples from the offshore U. K., *J. Struct. Geol.*, *18*, 155–167, 1996.

Öncel, A. O., I. Main, Ö. Aptekin, and P. A. Cowie, Spatial variations of the fractal properties of seimicity in the Anatolian fault zones, *Tectonophysics*, *257*, 189–202, 1996.

Peacock, D. C .P., R. J. Knipe, and D. J. Sanderson, Glossary of normal faults, *J. Struct. Geol.*, *22*, 291–305, 2000.

Ridcharson, M., and M. A. Arthur, The Gulf of Suez–nothern red sea Neogene rift: A quantitative basin analysis, *Mar. Pet. Geol.*, *5*, 247–270, 1988.

Schulz, S. E., and J. P. Evans, Spatial variability in microscopic deformation and composition of the Punchbowl Fault, southern California: Implications for mechanisms, fluid-rock interaction, and fault morphology, *Tectonophysics*, *295*, 223–244, 1998.

Schütz, K. I., Structure and stratigraphy of the Gulf of Suez, Egypt, *APPG Mem.*, *59*, 57–96, 1994.

Shipton, Z. K., and P. A. Cowie, Damage zone and slip-surface evolution over micrometre to kilometre scales in high-porosity Navajo sandstone, Utah, *J. Struct. Geol.*, *23*, 1825–1844, 2001.

Steckler, M. S., F. Berthelot, N. Lyberis, and X. LePichon, Subsidence in the gulf of Suez: Implications for rifting and plate kinematics, *Tectonophysics*, *153*, 249–270, 1988.

Steen, Ø., and A. Andresen, Effects of lithology on geometry and scaling of small faults in Triassic sandstones, East Greenland, *J. Struct. Geol.*, *21*, 1351–1368, 1999.

Underhill, J. R., and N. H. Woodcock, Faulting mechanisms in high-porosity sandstones; New Red Sandstone, Arra, Scotland, in *Deformation of Sediments and Sedimentary Rocks*, edited by M. E. Jones and R. M. F. Preston, *Geol. Soc. Spec. Publ.*, *29*, 91–105, 1987.

Vermilye, J. M., and C. H. Scholz, The process zone: A microstructural view of fault growth, *J. Geophys. Res.*, *103*, 12,223–12,237, 1998.

Vicsek, T., *Fractal Growth Phenomena*, 488 pp., World Sci., River Edge, N. J., 1989.

O. Bour, C. Darcel, and P. Davy, Géosciences Rennes (UMR6118), Campus de Beaulieu (Bat15), F-35042 Rennes cedex, France. (cdarcel@univ-rennes1.fr)

X. Du Bernard, Department of Geological and Environmental Sciences, Stanford University, Stanford, CA 94305-2115, USA. (xduberna@pangea.Stanford.edu)

P. Labaume, Laboratoire de Géophysique Interne et Tectonophysique (UMR 5559), BP 53X, F-38041 Grenoble cedex 9, France.